Aerothermodynamic and rotordynamic performance evaluation to diagnose deposits accumulation in a gas lift centrifugal compressor

Ahmed Al Mamari [*,1], Nasser Al Azri [**], Nabeel Al Rawahi

Department of Mechanical and Industrial Engineering, Sultan Qaboos University, Oman

ARTICLE INFO

ABSTRACT

The paper presents a case study focusing on the assessment of the aerothermodynamic and rotordynamic performance to diagnose deposit accumulation on the internals of a centrifugal compressor. The case involves a four-stage gas lift centrifugal compressor powered by a 5.9 MW induction motor and utilizing a fluid coupling to regulate the compressor's rotational speed. The Huntington 4-point method was employed to evaluate the polytropic head and efficiency of the four compressor sections over a 20-month period, with pressure and temperature data sampled every 6 hours. The efficiency model was supported by the GERG-2008 equation of state, used to calculate the necessary thermodynamic properties at intermediate and endpoint states. The aerothermodynamic analysis identified a deterioration in polytropic efficiency in compressor section 3, accompanied by a pressure drop and an increase in discharge temperature. Simultaneously, the rotordynamic response was examined through various vibration plots. Although the increase in the vibration amplitudes was not significant, a notable phase shift was observed. This decline in polytropic efficiency and change in vibration patterns were attributed to severe fouling, which was confirmed during the overhaul of the HP compressor. Root cause investigations revealed the deposit as reactive, leading to the installation of an online washing system. Over a nine-month observation period post-maintenance, the compressor operation was stable with no degradation in its polytropic efficiency.

Nomenclature

Parameters

c	Specific Heat Capacity
e	Polytropic Efficiency
P	Pressure
R	Gas Constant
s	Specific Entropy
T	Temperature
v	Specific Volume

* Corresponding author.
** Corresponding author.
E-mail addresses: S92349@student.squ.edu.om (A. Al Mamari), nalazri@squ.edu.om (N. Al Azri).
[1] First Author.

$\bar{x}$	Gas Composition Mole Fractions
y	Head
Z	Compressibility Factor
α	Dimensionless Helmholtz Free Energy
δ	Reduced Mixture Density
τ	Inverse Reduced Mixture Temperature

Subscripts and Superscripts

p	Polytropic
o	Ideal
r	Residual
1	Suction
2	Discharge

1. Introduction

Centrifugal compressors play a crucial role in the operations of any plant that involves gas processing. Hence, ensuring high reliability and availability of these critical pieces of equipment is essential for achieving the optimal productivity of the entire plant. Many mechanical and aerodynamic disturbances have the potential to adversely impact compressor reliability. Because these machines work with fluids, they are prone to fouling, which occurs due to the accumulation of deposits on the internal components of the compressor. Fouling exerts a detrimental impact on both the aerothermodynamic efficiency of the compressor and the rotor-dynamic response of the rotor-bearing system.

Concerning the impact on aerothermodynamic performance, fouling can deteriorate the compressor efficiency as it distorts the gas flow path, leading to the generation of irreversibilities such as turbulence, flow separation, and internal friction [1,2]. Consequently, the compressor may struggle to compress the gas to the desired pressure unless the flow is reduced, or the rotational speed is increased. Moreover, depending on the extent of irreversibilities, there can be a significant rise in the discharge temperature as well. It is noteworthy to point out that there are additional factors that can degrade the efficiency of the compressor. These include changes in the suction parameters, particularly pressure, temperature, and gas constituents, as well as damages to aerodynamic components like the impeller and diffuser [3,4]. Therefore, diagnosing compressor fouling goes beyond assessing the polytropic efficiency alone. Indeed, for a thorough evaluation, it is essential to correlate the calculated head and efficiency with various parameters like flow, speed, anti-surge valve position, as well as suction and discharge parameters. This comprehensive approach provides a more accurate understanding of the system's aerothermodynamic performance.

Likewise, fouling can perturb the rotordynamic response of the machine. It can cause the rotor dynamic response to undergo increased amplitudes and phase shifts stemming from changes in both the magnitude and location of the unbalance force. The impact of this synchronous dynamic force can be critical, particularly in cases of low damping ratio, resulting in increased vibration amplitudes and potential machine tripping. Furthermore, when these dynamic forces reach significant levels, the response can pose a threat to the machine. High relative shaft vibration may result in physical contact between rotating and stationary components. Likewise, high vibration amplitudes imply increased cyclic loads on the rotor-bearing system. If the compressor operates consistently at high vibration amplitudes and under substantial cyclic loads, it could potentially result in fatigue failure over time.

The deposit accumulation on the compressor internals can be classified into two categories: non-reactive and reactive deposit accumulation [5]. Non-reactive deposits refer to foreign materials that contaminate the compressed gas, passing through the inlet filters and adhering to the compressor internals without changing their physical state. This includes dust, scale, and catalyst fine [5]. Non-reactive deposits can be simply avoided by making the right selection of the filters upstream the compressor inlet. In contrast to non-reactive deposits, reactive deposits enter the compressor in gaseous form, undergoing a change in physical state as they undergo compression within the compressor stages. Hence, mitigating the risk of reactive deposits involves methods beyond the selection of the inlet filters. One such approach is the installation of online washing systems that inject specific substances to prevent deposit formation in the compression stages [6].

This paper presents a case study focused on diagnosing deposit accumulation in a motor-driven gas lift compressor. The evaluation of the aerothermodynamic performance involved calculating the compressor polytropic head and efficiency and correlating their trends with various process parameters. Additionally, the rotordynamic response was examined by analyzing the relative shaft vibration patterns through the diagnostic plots such as time waveforms, orbit, polar, and spectrum plots.

2. Compressor efficiency

Unlike the conventional definition of efficiency, which measures the useful extracted work against the supplied energy, compression efficiency is typically computed using the second law efficiency principle. The second law of thermodynamics acknowledges that energy possesses both quality and quantity. Consequently, there exists an ideal work path that assumes the minimum work required to transition from the suction state to the discharge state with minimal losses. As a result, compression efficiency is defined as the ratio of the ideal work to the actual work transferred to the gas [7]. The ideal work can generally take the form of isothermal, isentropic, or polytropic processes. In the isothermal process, heat is continuously removed during compression to maintain a constant temperature. However, this approach is generally not practical. On the other hand, isentropic work assumes an adiabatic and reversible com-

pression process, where entropy generation is zero due to the absence of irreversibilities. The widely adopted method for assessing compressor efficiency is the polytropic efficiency. This approach offers a robust means of comparing compressors with the same aerodynamic design, even if they have different pressure ratios. The polytropic work accounts for maximum cooling, disregarding the impact of preheating, and focuses solely on other irreversibilities like turbulence, flow separation, and friction [2].

Applying the first law of thermodynamics to the compressor control volume reveals that the actual work is equivalent to the enthalpy difference between the discharge and suction states. It is important to emphasize that this is valid only when assuming an adiabatic process and neglecting changes in kinetic and potential energy. Consequently, determining the actual work is a straightforward process using a real gas equation of state. The first trial to develop a PVT model for real gasses was by Van Der Waals in 1873 [8]. Subsequently, numerous models have been devised for the modeling of both pure substances and mixtures. Lüdtke [2] conducted a comparison among four widely employed equations of state in the gas industry. These four models, which are based in the corresponding state principle, are outlined as follows.

1. **BWRS:** A virial-type equation of state initially published by Benedict, Webb, and Rubin in 1940 and subsequently modified by Starling in 1973 [9,10].
2. **RKS:** A cubic equation of state proposed by Redlich and Kwong in 1949 and later enhanced by Soave in 1972 [11,12].
3. **LKP:** A virial-type equation of state introduced by Lee and Kesler in 1975, with modifications in 1978 by Knapp, Plocker, Plocker, and Prausnitz [13,14]. This equation is one of the most commonly used among the compressor manufactures.
4. **Peng Robinson:** A cubic equation of state developed by Peng and Robinson in 1976 [15]. This equation evolved from the Van Der Waals equation.

Another class of PVT models appeared later which characterize the mixture behavior by utilizing excess properties. Despite their complexity, equations of state falling into this category often exhibit higher accuracy. The AGA8-DC92 equation is a notable example of this type. This model is explicit in Helmholtz free energy, and it was initially introduced by Starling and Savidge in 1992 [16]. The AGA8-DC92 is adopted by ISO20765-1, and it is used for natural gas mixtures that consist of up to 21 substances [17]. GERG-2008 is another example of equations of state that are explicit in Helmholtz energy. Initially known as GERG-2004, this model was utilized for calculating the thermodynamic properties of natural gas mixtures with up to 18 components [18]. The GERG model underwent modifications later to incorporate three additional substances, evolving into GERG-2008 [19]. Despite its complexity, this model is employed in this study for calculating the necessary thermodynamic properties due to its high level of accuracy.

The polytropic head is defined by equation (1). Because work is a path-dependent quantity, numerous models have been developed to estimate the polytropic path and enhance integral evaluation. These methods generally fall into two categories: end-point methods and stepped integral methods. End-point models solely rely on suction and discharge thermodynamic properties, calculated using an equation of state. Conversely, stepped integral methods are essentially numerical approaches that aim to evaluate the integral by dividing it into multiple steps and conducting iterative calculations, requiring assumptions for thermodynamic properties at each step [20,21]. conducted comprehensive comparisons of methods falling under both categories. In general, stepped integral methods offer greater accuracy, albeit at the expense of increased complexity and computational power. Table 1 presents a concise overview of the most prevalent approaches. In this study, the Huntington 4-Point method is employed to model the polytropic head and efficiency, with the support of the GERG-2008 equation of state for calculating the thermodynamic properties.

$$y_p = \int_1^2 v \, dP \tag{1}$$

3. Methodology

According to Huntington 4-Point method, the entropy difference between the suction and discharge is given by equation (2):

$$(s_2 - s_1) = R \frac{(l-e)}{e} \left\{ a \cdot \ln \frac{P_2}{P_1} + b \cdot \left(\frac{P_2}{P_1} - 1 \right) + \frac{c}{2} \left(\ln \frac{P_2}{P_1} \right)^2 + d \cdot \left[\frac{P_2}{P_1} \ln \frac{P_2}{P_1} - \left(\frac{P_2}{P_1} - 1 \right) \right] \right\} \tag{2}$$

The coefficients a, b, c, and d are calculated by solving equations (3)–(6) simultaneously:

$$Z_1 = a + b \tag{3}$$

Table 1
Polytropic head and efficiency calculation methods.

End Point Methods	Stepped Numerical Methods
Schultz [22,23]	Huntington Reference [24]
Mallen and Saville [25]	Small Stage [26]
Sandberg and Colby [27]	Sandberg and Colby Reference [27]
Schultz XY (2&3 Point) [22]	Nathoo and Gottenberg [28]
Huntington 3 Point [24]	Oldrich [29]
Huntington 4 Point [21]	Wettstein [30]
Taher–Evans Cubic Polynomial (TE-CP) [31]	Huntington 2017 Reference [21]

$$Z_2 = a + b\left(P_2/P_1\right) + c\ \ln\ \left(P_2/P_1\right) + d\left(P_2/P_1\right)\ln\ \left(P_2/P_1\right) \tag{4}$$

$$Z_3 = a + b\left(P_3/P_1\right) + c\ \ln\ \left(P_3/P_1\right) + d\left(P_3/P_1\right)\ln\ \left(P_3/P_1\right) \tag{5}$$

$$Z_4 = a + b\left(P_4/P_1\right) + c\ \ln\ \left(P_4/P_1\right) + d\left(P_4/P_1\right)\ln\ \left(P_4/P_1\right) \tag{6}$$

The pressure and temperature of the two intermediate states are estimated by equations (7)–(10):

$$P_3 = \left(\frac{P_2}{P_1}\right)^{1/3} \tag{7}$$

$$P_4 = P_1\left(\frac{P_2}{P_1}\right)^{2/3} \tag{8}$$

$$T_3 = T_1\left(P_3/P_l\right)^m \tag{9}$$

$$T_4 = T_1\left(P_4/P_l\right)^m \tag{10}$$

Where: $m = \ln\ \left(T_2/T_l\right)/\ln\ \left(P_2/P_l\right)$.

The anticipated entropy values for the intermediate states are determined through equations (11) and (12). Subsequently, these calculated entropy values are compared with the entropy computed from the equation of state using the previously estimated pressure and temperature at the intermediate states.

$$s_3' = s_1 + R\frac{(1-e)}{e}\left\{a\ \ln\ \left(P_3/P_1\right) + b\left[\left(P_3/P_1\right) - 1\right] + \frac{c}{2}\left[\ln\ \left(P_3/P\right)\right]^2 + d\left[\left(P_3/P_1\right)\ln\ \left(P_3/P_1\right) - \left(P_3/P_1\right) + 1\right]\right\} \tag{11}$$

$$s_4' = s_1 + R\frac{(1-e)}{e}\left\{a\ \ln\ \left(P_4/P_1\right) + b\left[\left(P_4/P_1\right) - 1\right] + \frac{c}{2}\left[\ln\ \left(P_4/P_1\right)\right]^2 + d\left[\left(P_4/P_1\right)\ln\ \left(P_4/P_1\right) - \left(P_4/P_1\right) + 1\right]\right\} \tag{12}$$

Improved estimations of temperature at the intermediate states can now be calculated using equations (13) and (14).

$$T_3' = T_3\ \exp\ \left[\left(s_3' - s_3\right)/C_{p,3}\right] \tag{13}$$

$$T_4' = T_4\ \exp\ \left[\left(s_4' - s_4\right)/C_{p,4}\right] \tag{14}$$

The GERG-2008 model is employed for computing entropy, specific heats, and the compressibility factor, as outlined in equations (15)–(17). It is important to highlight that the GERG-2008 model is designed to accept density and temperature as inputs, whereas the available properties are pressure and temperature. To address this, the secant method was employed for solving the equation of state.

$$\frac{s\left(\delta, \tau, \bar{x}\right)}{R} = \tau\left(\alpha_\tau^o + \alpha_\tau^r\right) - \alpha^o - \alpha^r \tag{15}$$

$$\frac{c_p\left(\delta, \tau, \bar{x}\right)}{R} = -\tau^2\left(\alpha_{\tau\tau}^o + \alpha_{\tau\tau}^r\right) + \frac{\left(1 + \delta\alpha_\delta^r - \delta\tau\alpha_{\delta\tau}^r\right)^2}{1 + 2\delta\alpha_\delta^r + \delta^2\alpha_{\delta\delta}^r} \tag{16}$$

$$Z\left(\delta, \tau, \bar{x}\right) = 1 + \delta\alpha_\delta^r \tag{17}$$

The prescribed process is reiterated using the newly estimated temperatures, and this cycle is repeated until the entropies at the intermediate states converge. It is worth noting that the validation of the described procedure has been addressed in a previous publication and is beyond the scope of the current work [32].

4. Machine train design and configuration

The diagram in Fig. 1 illustrates the setup of the machine train studied in this case. The prime mover is an induction motor, boasting a rated power and speed of 5.9 MW and 1487 rpm, respectively. The transmission system is Voith Vorecon, RWE type, which comprises a fluid coupling (torque converter) and a planetary gear set. The speed of the compressor is regulated by adjusting the superimposing speed of the planet gears' carrier. This adjustment is achieved by changing the position angle of the adjustable guide vanes of the torque converter, facilitating torque conversion through the fluid between the pump and turbine impellers.

Furthermore, the machine train includes two compressor casings: LP and HP. The LP casing consists of two sections, each featuring four compression stages (four impellers). The impellers of the two sections in the LP casing are arranged in a back-to-back configuration. Likewise, the HP casing is composed of two sections, each hosting four compression stages. In contrast to LP, the impellers arrangement in HP compressor is straight-through configuration.

Flexible couplings are employed as connections between all the rotors in the machine train except between the low-speed and high-speed rotors in the transmission system which are connected through the torque converter and the planetary gear set for the pur-
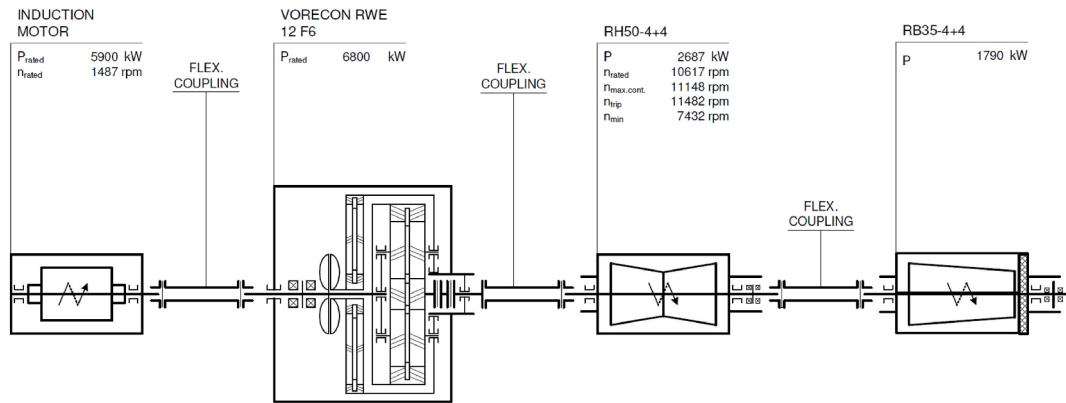
Fig. 1. Machine train Configuration.

pose of regulating the compressor rotational speed. Additionally, all five rotors are supported by fluid film hydrodynamic bearings. The shaft relative vibration of both compressor rotors is monitored using two orthogonal and coplanar proximity sensors at each bearing plane.

In this study, each compressor section is considered a standalone entity. Consequently, the analysis procedure outlined in the methodology section is implemented independently on each of the four individual sections. General aerodynamic design parameters are provided in Tables 2–4 below.

5. Results and discussion

The analysis procedure detailed in the methodology section was executed independently for each section. Data on suction and discharge pressure, as well as temperature, were gathered over a 20-month period. To ensure accuracy and prevent unrealistic efficiency

Table 2
General design parameters.

Parameter	LP Casing		HP Casing	
	Section 1	Section 2	Section 3	Section 4
$\dot{Q}$ (MSm^3/d)	607	601	587	577
$\dot{m}$ (kg/h)	27,817	27,630	26,664	25,654
n (rpm)	10,299			
h_p (Nm/kg)	131,947	116,506	68,833	62,593
η_p (%)	83	71.8	67.9	58.6

Table 3
Design suction parameters.

Parameter	LP Casing		HP Casing	
	Section 1	Section 2	Section 3	Section 4
P_s (barA)	2.7	8.021	21.4	39.8
T_s (°C)	48	60	60	60
MW_s (kg/kmol)	26	26.08	25.76	25.25
Z_s	0.99	0.975	0.937	0.888
C_p/C_v	1.197	1.186	1.253	1.329

Table 4
Design discharge parameters.

Parameter	LP Casing		HP Casing	
	Section 1	Section 2	Section 3	Section 4
P_d (barA)	8.62	22	40.4	72
T_d (°C)	127	140.6	112.6	113.3
Z_d	0.986	0.97	0.933	0.9
C_p/C_v	1.167	1.161	1.252	1.322

calculations, erroneous data and downtime periods were excluded from the analysis. A sampling rate of one sample every six hours was established to mitigate aliasing resulting from fluctuations in ambient conditions. Consequently, the described analysis was performed approximately 3600 times for each section to produce polytropic head and efficiency trends. On average, the software took around 15 minutes to generate the trends for polytropic head and efficiency in each section. That is, one hour for the entire compressor train. The software was run using 11th Gen Intel(R) Core (TM) i7-11850H @ 2.50 GHz.

The trends for polytropic head and efficiency in sections 1,2, and 4 were observed to be consistent and exhibited strong correlations with other process parameters, including flow rate, speed, ASV opening, pressure, and temperature. Figs. 2–4 depict the calculated polytropic head and efficiency throughout the investigation period.

Nevertheless, section 3 displayed a significant decrease in the calculated polytropic efficiency and head. Fig. 5 depicts the calculated polytropic head and efficiency for section 3. It is obvious from the trend that the polytropic efficiency experienced a drop of around 20%, while the polytropic head showed a decline of approximately 10 kJ/kg. This reduction in polytropic head and efficiency coincided with an increase in discharge temperature, signaling increased internal irreversibilities likely caused by friction and flow disturbances. In the meantime, minor drop in discharge pressure, around 2 bar, was also observed. The discharge pressure and temperature of section 3 are presented in Fig. 6.

Additionally, the decline in discharge pressure was coupled with a reduction in mass flow rate, approximately 1 kg/s at the same speed. Consequently, there was a necessity to operate the compressor at a relatively higher speed to augment the mass flow rate at a specified pressure. The trends for flow and speed are illustrated in Fig. 7.

After the thermodynamic analysis, the rotordynamic response was also examined. Fig. 8 illustrates the unfiltered vibration amplitudes for DE and NDE bearings of the HP compressor. It is evident from the figure that vibration amplitudes have doubled, increasing from 5 μm to 10 μm. However, this increment is deemed insignificant considering the bearing clearance is 80 μm, and it is also taken into account that the compressor had to operate at a higher speed to achieve the required throughput. Upon closer inspection, it was noted that the measured phase angle had shifted by approximately 120°. Spectrum, time waveform, and orbit plots (see Figs. 9, 10, 11
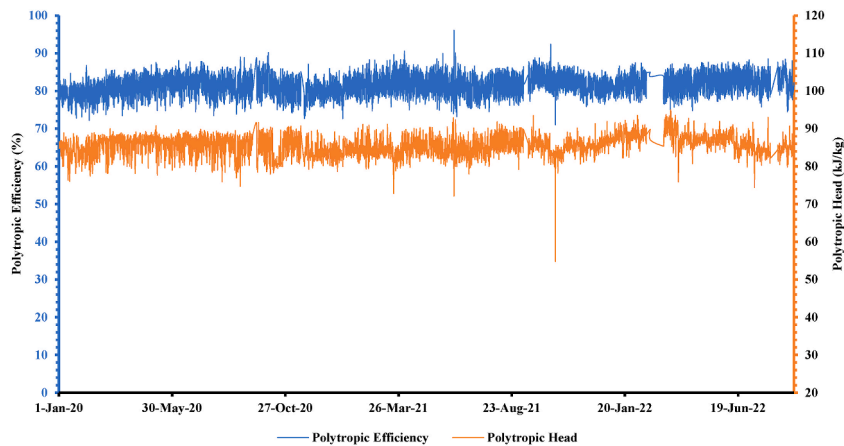

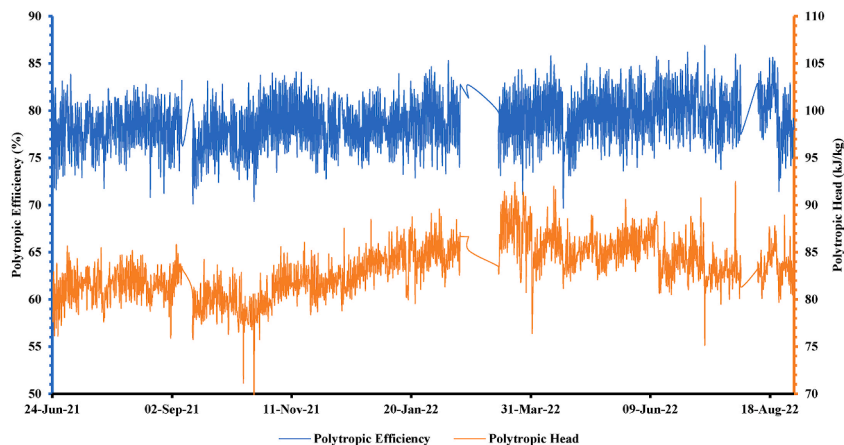**Fig. 2.** Calculated polytropic head and efficiency for Section 1.

Fig. 3. Calculated polytropic head and efficiency for Section 2.
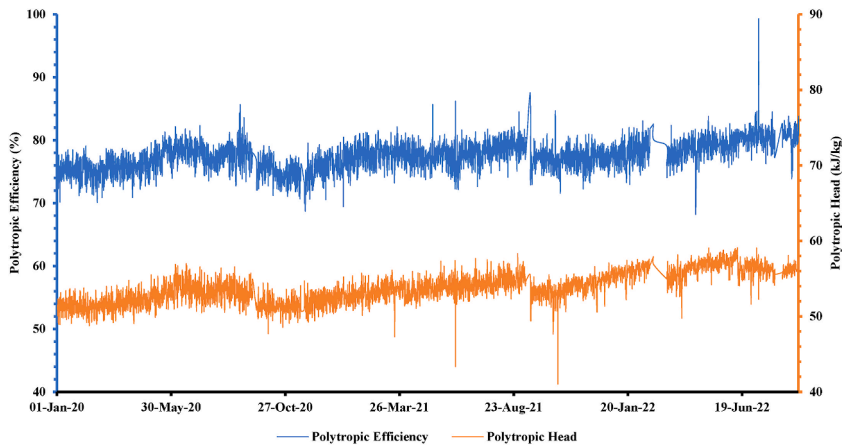
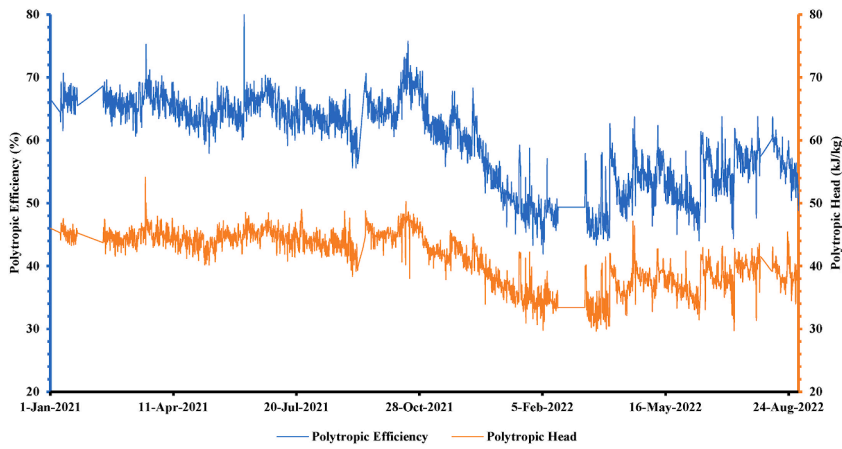**Fig. 4.** Calculated polytropic head and efficiency for Section 4.

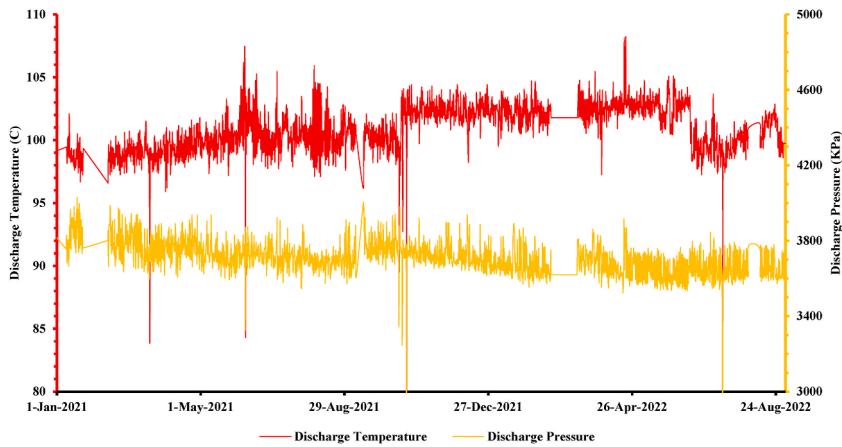**Fig. 5.** Calculated polytropic head and efficiency for Section 3.

Fig. 6. Section 3 Discharge parameters.

and 12) clearly indicated that the vibration is purely synchronous, with no indications of any mechanical malfunction. Hence, the phase angle shift can be attributed to deposits adhering to the rotor.

The slight increase in vibration amplitude can be ascribed to the short rotor span and the high damping in this rotor-bearing system. However, the shift in phase angle clearly signals a change in the location of the synchronous dynamic forces acting on the rotor bearing system, particularly in the absence of any mechanical malfunction indications (see Fig. 12).
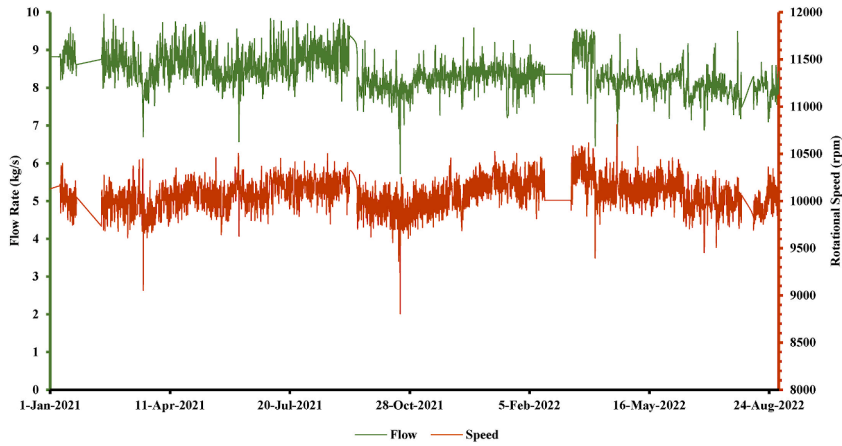
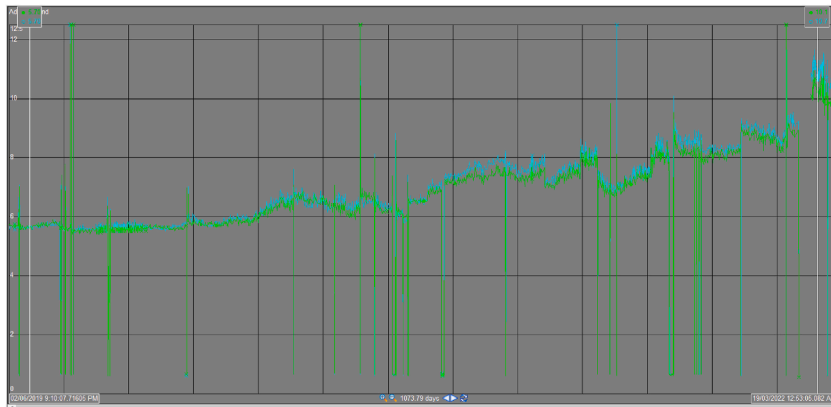**Fig. 7.** Mass flow rate and rotational speed trends in section 3.

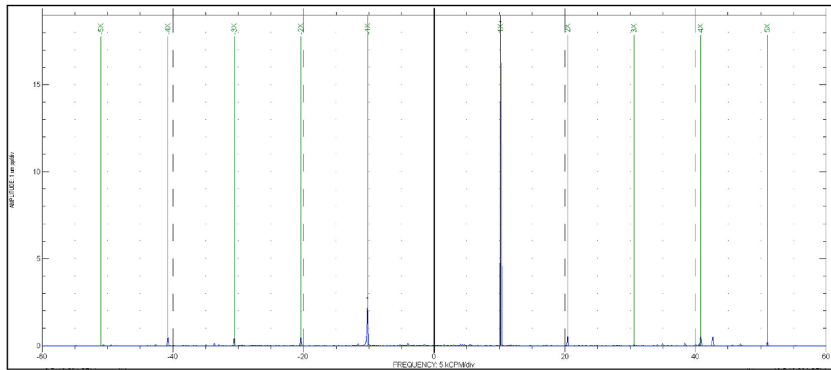**Fig. 8.** Unfiltered shaft vibration response the HP compressor DE and NDE bearings.

Fig. 9. DE Full spectrum.

In consideration of the above analysis and results, the decision was made to overhaul the HP compressor. Fig. 13 provides a visual of the HP internals, with significant fouling evident in section 3 on the right-hand side, particularly at the first and second stages (see Fig. 14).

Following this, a root cause analysis was conducted, indicating that the fouling issue originated from a temperature drop downstream of the intercooler, caused by specific process disturbances. Additionally, the inlet filter design was revised, and an online washing system was installed. Subsequently, the aerothermodynamic performance of the compressor was monitored. Fig. 15 depicts the trends in polytropic head and efficiency after nine months of operation post-overhauling. Clearly visible from Fig. 15 is the improved stability in the compressor performance, underscoring an enhancement in the compressor's reliability.
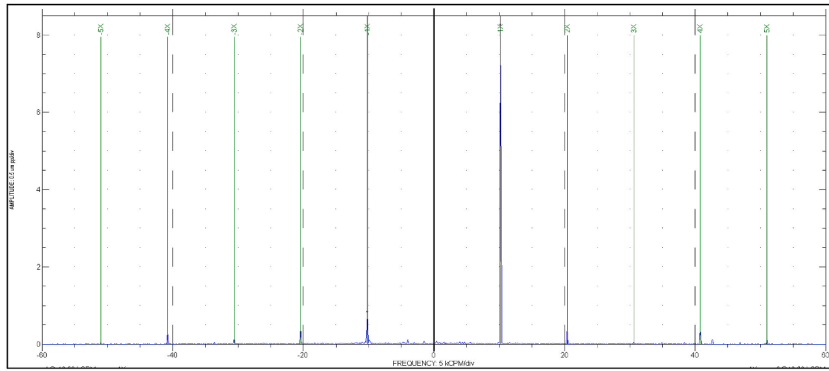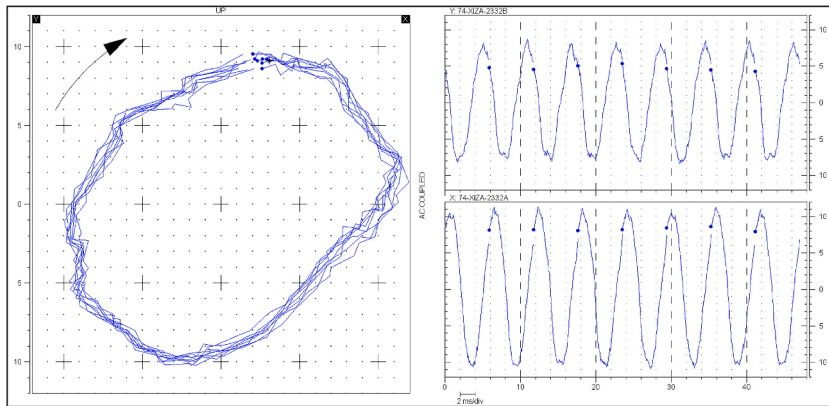
Fig. 10. NDE Full spectrum.

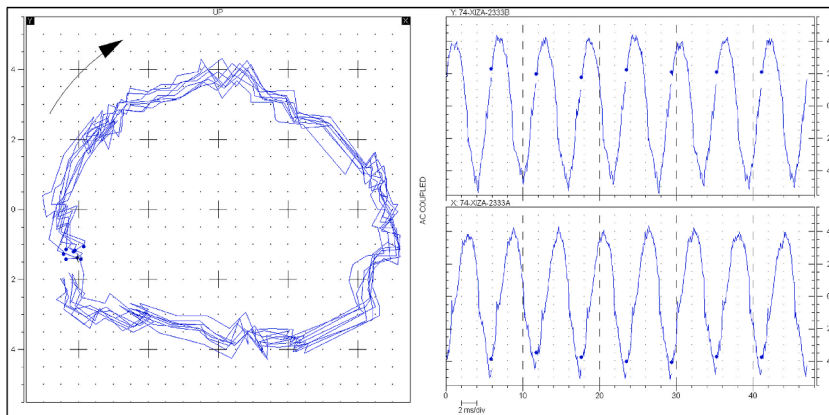**Fig. 11.** DE unfiltered orbit and time waveforms.

Fig. 12. NDE unfiltered orbit and time waveforms.

6. Conclusion and recommendations

The paper outlined a systematic approach for assessing the aerothermodynamic performance of centrifugal compressors in industrial processes. The methodology was applied to a 5.9 MW motor-driven gas lift compressor. Notably, a substantial decline in polytropic head and efficiency was identified in section 3 of the HP compressor. This decline was accompanied by abnormal correlations with other process parameters. Additionally, an examination of the rotordynamic response of the compressor train was conducted confirming the absence of any mechanical malfunctions. The HP compressor underwent a major overhaul, revealing substantial fouling in section 3, particularly in the first two impellers.

Despite the minor increase in shaft vibration amplitudes, a significant shift of around 120° in phase angle indicated a notable displacement of synchronous dynamic forces. Therefore, it is recommended to develop rotordynamic models for various compressor sizes and geometries to investigate the factors influencing the impact of deposit accumulation on the magnitude of rotordynamic re-
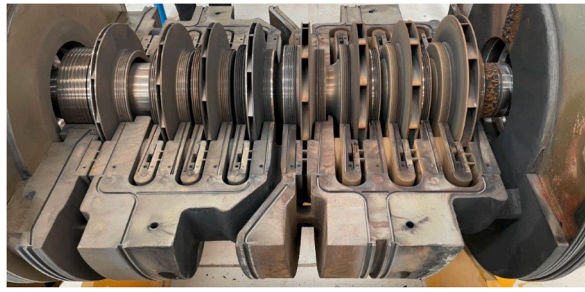
Fig. 13. HP compressor.
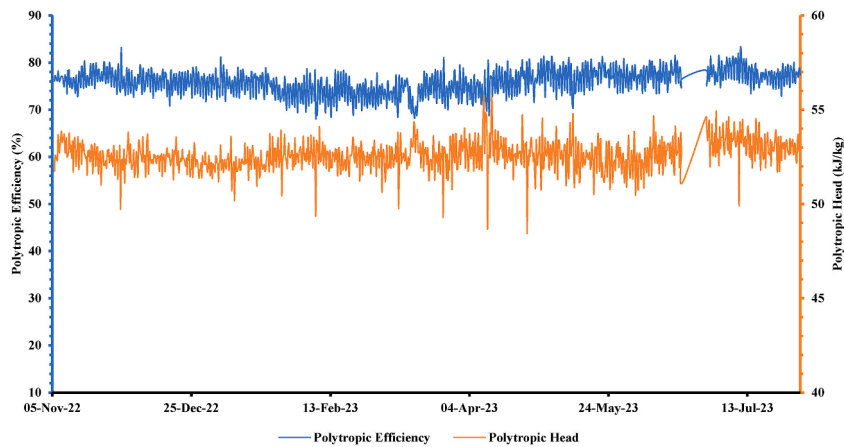

Fig. 14. First stage in Section 3.

Fig. 15. Polytropic head and efficiency post overhauling.

sponses. Furthermore, it is advisable to develop models capable of predicting theoretical efficiency, head, discharge pressure, and temperature. These predictions can serve as benchmarks for evaluating compressor performance. Attaining this objective might include employing both first-principle physics models, known for their high accuracy, and exploring the option of AI models. However, the latter approach demands a substantial amount of high-quality historical data to be input into diverse AI models for observation and analysis of the outcomes.

Likewise, it is advisable to create models capable of predicting the current compressor performance maps using the present inlet parameters, as-tested maps, and conditions as inputs to generate the equivalent maps. Implementing such models to a reactive control system would prove highly beneficial for optimizing compressor operation and minimizing energy consumption.

CRediT authorship contribution statement

Ahmed Al Mamari: Conceptualization, Data curation, Formal analysis, Investigation, Methodology, Software, Validation, Visualization, Writing – original draft. **Nasser Al Azri:** Funding acquisition, Software, Writing – review & editing, Supervision. **Nabeel Al Rawahi:** Funding acquisition, Supervision.

Declaration of competing interest

The authors declare that they have no known competing financial interests or personal relationships that could have appeared to influence the work reported in this paper.

Data availability

The data that has been used is confidential.

Acknowledgement

References

[1] Y.a.a.M.A. Boles, Thermodynamics: an Engineering Approach, McGraw-Hill Education, New York, 2015.
[2] K. Lüdtke, Process Centrifugal Compressors, Springer-Verlag, Berlin, 2004.
[3] M.T. Gresh, Compressor Performance: Aerodynamics for the User, second ed., Newnes, London, 2001.
[4] W. Al Busaidi, P. Pilidis, Investigation of efficiency deterioration causes in process centrifugal compressor operation, J. Fail. Anal. Prev. 16 (2016) 19–36.
[5] W. Al-Busaidi, P. Pilidis, Modelling of the non-reactive deposits impact on centrifugal, Engineering Failuire Analysis 60 (2015) 57–85.
[6] A. Watson, D. Carter, C. Alleyne, Cleaning turbomachinery without disassembly, online and offline, in: Twenty-Fourth Turbomachinery Symposium, 1995.
[7] M. Casey, C. Rhobinson, Radial Flow Turbocompressors: Design, Analysis, and Applications, Cambridge University Press, Cambridge, 2021.
[8] J.D.v. d. Waals, de Continuiteit van den Gas- en Vloeistoftoestand2, University of Leiden, Leiden, 1873.
[9] M. Benedict, G.B. Webb, Rubin, C. Louis, An empirical equation for thermodynamic properties of light hydrocarbons and their mixtures i. Methane, ethane, propane and n-butane, J. Chem. Phys. 8 (1940) 334–345.
[10] K.E. Starling, J.E. Powers, Enthalpy of mixtures by modified BWR equation, Ind. Eng. Chem. Fundam. 9 (1973) 531–537.
[11] O. Kowng, J. Redlich, On the thermodynamics of solutions; an equation of state; fugacities of gaseous solutions, Chem. Rev. 44–1 (1949) 233–244.
[12] G.S. Soave, Equilibrium constants from a modified redlich-kwong equation of state, Chem. Eng. Sci. 27 (1972) 1197–1203.
[13] B.I. Lee, M.G. Kesler, A generalized thermodynamic correlation based on three-parameter corrosponding states, AIChE J. 21 (3) (1975) 510–527.
[14] H.K.a.J.P. Uif Plöcker, Calculation of high-pressure vapor-liquid equilibria from a corrosponding-states correlation with emphasis on asymmetric mixtures, Ind. Eng. Chem. Process Des. Dev. 17 (1978) 324–332.
[15] D. Peng, D. Robinson, A new two-constant equation of state, Ind. Eng. Chem. Fundam. 15 (1976) 59–64.
[16] Starling and Savidge, Compressibility Factors of Natural Gas and Other Related Hydrocarbon Gases, American Gas Association, 1992.
[17] ISO, ISO20765-1: Natural Gas-Calculation of Thermodynamic Properties Part 1: Gas Phase Properties for Transmission and Distribution, 2005 Geneva.
[18] O. Kunz, R. Klimeck, W. Wagner, M. Jaeschke, The GERG-2004 Wide-Range Equation of State for Natural Gases and Other Mixtures, VDI Verlag GmbH, Düsseldorf, 2007.
[19] W. Wagner, O. Kunz, The GERG-2008 wide-range equation of state for natural gases and other mixtures: an expansion of GERG-2004, J. Chem. Eng. Data 57 (2012) 3032–3091.
[20] F. Evans, S. Huble, Centrifugal compressor performance making enlightened analysis decisions, in: 46th Turbomachinery and 33rd Pump Symposia, 2017 Houston.
[21] R.A. Huntington, Another new look at polytropic calculations methods for turbomachinery, Research Gate (2017).
[22] J.M. Schultz, The polytropic analysis of centrifugal compressors, Journal of Engineering for Power 84 (1962) 69–82.
[23] ASME PTC-10, American Society of Mechanical Engineers, New York, 1997.
[24] R.A. Huntington, Evaluation of polytropic calculation methods for turbomachinery performance, Journal of Engineering for Gas Turbines and Power-Transactions of the Asme 107 (1985) 872–876.
[25] M.M.a.G. Saville, Polytropic Processes in the Performance Prediction of Centrifugal Compressors, Institution of Mechanical Engineers, 1977, pp. 89–96.
[26] O. Hundseid, L.E. Bakken, T. Helde, A revised compressor polytropic performance analysis, in: Roceedings of ASME GT2006, 2006.
[27] M.S.a.G.M. Colby, Limitations of ASME PTC 10 in accurately evaluating centrifugal compressor thermodynamic performance, in: Forty-Second Turbomachinery Symposium, 2013 Houston.
[28] N.S. Nathoo, W.G. Gottenberg, A new look at performance analysis of centrifugal compressors operating with mixed hydrocarbon gases, Journal of Engineering for Power 105 (1983) 920–926.
[29] Oldřich, Advanced polytropic calculation method of centrifugal compressor, in: ASME International Mechanical Engineering Congress and Exposition 2010, 2010.
[30] H.E. Wettstein, Polytropic change of state calculations, in: International Mechanical Engineering Congress and Exposition 2014, 2014.
[31] M. Taher, F. Evans, Centrifugal compressor polytropic performance—improved rapid calculation results—cubic polynomial methods, International Journal of Turbomachinery Propulsion and Power (2021).
[32] A. Al Mamari, N. Al Azri, N. Al Rawahi, A thermodynamic approach to the enhancement of reliability and the optimization of energy efficiency of centrifugal compressors, in: Abu Dhabi International Petroleum Exhibition and Conference, 2023 Abu Dhabi.